AFRL-RW-EG-TP-2010-111

Shock Equation of State of Multi-Phase Epoxy-Based Composite (Al-MnO_2-Epoxy)

Authors: See enclosed paper

Performing Organizations: See enclosed paper

October 2010

Interim Report for Period October 2008 – October 2009

AIR FORCE RESEARCH LABORATORY, MUNITIONS DIRECTORATE

Air Force Materiel Command ■ United States Air Force ■ Eglin Air Force Base

NOTICE AND SIGNATURE PAGE

AFRL-RW-EG-TP-2010-111 HAS BEEN REVIEWED AND IS APPROVED FOR PUBLICATION IN ACCORDANCE WITH ASSIGNED DISTRIBUTION STATEMENT.

FOR THE DIRECTOR:

//ORIGINAL SIGNED//	//ORIGINAL SIGNED//	//ORIGINAL SIGNED//
HOWARD G. WHITE, PhD	JEFFREY D. KUHN, MAJ, PhD	JENNIFER L. JORDAN, PhD
Technical Advisor	Branch Chief	Project Manager
Ordnance Division	Energetic Materials Branch	Energetic Materials Branch

REPORT DOCUMENTATION PAGE

Form Approved
OMB No. 0704-0188

1. REPORT DATE *(DD-MM-YYYY)*	**2. REPORT TYPE**	**3. DATES COVERED** *(From - To)*
10-2010	Interim	October 2008 – October 2009

4. TITLE AND SUBTITLE

Shock Equation of State of Multi-Phase Epoxy-Based Composite (Al-MnO_2-Epoxy)

5a. CONTRACT NUMBER

5b. GRANT NUMBER

5c. PROGRAM ELEMENT NUMBER
61102F

6. AUTHOR(S)

See enclosed presentations

5d. PROJECT NUMBER
2302

5e. TASK NUMBER
DW

5f. WORK UNIT NUMBER
90

7. PERFORMING ORGANIZATION NAME(S) AND ADDRESS(ES)

Air Force Research Laboratory, Munitions Directorate
Ordnance Division
Energetic Materials Branch (AFRL/RWME)
Eglin AFB FL 32542-5910
Technical Advisor: Dr. Jennifer L. Jordan

8. PERFORMING ORGANIZATION REPORT NUMBER

AFRL-RW-EG-TR-2010-111

9. SPONSORING / MONITORING AGENCY NAME(S) AND ADDRESS(ES)

Air Force Research Laboratory, Munitions Directorate
Ordnance Division
Energetic Materials Branch (AFRL/RWME)
Eglin AFB FL 32542-5910

10. SPONSOR/MONITOR'S ACRONYM(S)
AFRL-RW-EG

11. SPONSOR/MONITOR'S REPORT NUMBER(S)
Same as Block 8

12. DISTRIBUTION / AVAILABILITY STATEMENT

Distribution A: Approved for public release; distribution unlimited. Approval Confirmation 96 ABW/PA # 96ABW-2009-0300 29 June 2009

13. SUPPLEMENTARY

14. ABSTRACT

There are several studies in the literature regarding the equation of state of alumina-epoxy composites. Although these single component systems interact in a complex manner with shock waves, the addition of a second metal or ceramic particulate can result in even more complex interactions. This paper presents the shock equation of state results on a multi-phase composite Al–MnO2-epoxy. Equation of state experiments were conducted using three different loading techniques—single stage light gas gun, two stage light gas gun, and explosive loading—with multiple diagnostic techniques. The *Us−up* relationship is shown to be linear, with deviations from linearity at low, and possibly high, pressures due to the behavior of the epoxy binder. The experimental equation of state data is compared to volume averaged and mesoscale mixture models.

15. SUBJECT TERMS
Equation of state, Hugoniot, particulate composite, mixture model

16. SECURITY CLASSIFICATION OF:			**17. LIMITATION OF ABSTRACT**	**18. NUMBER OF PAGES**	**19a. NAME OF RESPONSIBLE PERSON**
a. REPORT	**b. ABSTRACT**	**c. THIS PAGE**			Jennifer L. Jordan
UNCLASSIFIED	UNCLASSIFIED	UNCLASSIFIED	UL	15	**19b. TELEPHONE NUMBER** *(include area code)* 850-882-8992

Shock equation of state of a multi-phase epoxy-based composite (Al–MnO_2-epoxy)

Jennifer L. Jordan,[1,a)] Dana M. Dattelbaum,[2] Gerrit Sutherland,[3] D. Wayne Richards,[1] Stephen A. Sheffield,[2] and Richard D. Dick[4]
[1]*Munitions Directorate, Air Force Research Laboratory (AFRL/RWMED), Eglin AFB, Florida 32542, USA*
[2]*Los Alamos National Laboratory, Los Alamos, New Mexico 87545, USA*
[3]*Naval Surface Warfare Center, Indian Head, Maryland, 20640USA*
[4]*Shocks Unlimited, Albuquerque, New Mexico, USA*

(Received 2 November 2009; accepted 5 February 2010; published online 26 May 2010)

There are several studies in the literature regarding the equation of state of alumina-epoxy composites. Although these single component systems interact in a complex manner with shock waves, the addition of a second metal or ceramic particulate can result in even more complex interactions. This paper presents the shock equation of state results on a multi-phase composite Al–MnO_2-epoxy. Equation of state experiments were conducted using three different loading techniques—single stage light gas gun, two stage light gas gun, and explosive loading—with multiple diagnostic techniques. The U_s-u_p relationship is shown to be linear, with deviations from linearity at low, and possibly high, pressures due to the behavior of the epoxy binder. The experimental equation of state data is compared to volume averaged and mesoscale mixture models. © *2010 American Institute of Physics*. [doi:10.1063/1.3357314]

I. INTRODUCTION

Filled polymers are often used in applications in which they are stressed or subjected to temperature variations. Polymer-filler interactions provide improved material strength and integrity in these applications. Filled epoxy composites are an attractive class of filled polymers used in structural components as they are lightweight, inexpensive, and easy to formulate, with tunable properties based on polymer-to-filler ratios and epoxy chemistry.

The shock response of polymers has been studied in detail,[1] including the shock properties of epoxy.[1–6] There are a couple of features of the shock response that are common to most polymers. Carter and Marsh[1] observed that a linear Rankine–Hugoniot fit to the Hugoniot data in the shock velocity-particle velocity (U_s-u_p) plane extrapolates to a value above the bulk sound velocity determined from ultrasound. They attribute this difference to disparate intermolecular and intramolecular forces, with the spacing between the polymer chains decreasing while the chain length remains relatively constant. Second, Carter and Marsh[1] also observed a high pressure (23.1 GPa for epoxy) break in slope in the Hugoniot in shock velocity-particle velocity for all of the polymers they studied, with the magnitude of the cusp related to chemical structure. The large volume changes associated with this transition point was assigned to interchain chemistry, with the volume collapse proportional to the size of the polymer side groups. Related studies shocking polymers above this cusp indicate possible decomposition of the polymer at even higher pressures.[7,8] Comparison of the shock response several similar epoxy systems[1,3–6] reveals that variations in epoxy composition have little effect on the Hugoniot behavior, at least in the measured pressure regimes. In general, the Hugoniot of epoxy over the range of pressure associated with the unreacted polymer can be represented in the shock velocity-particle velocity plane by $U_s = 2.69 + 1.51 * u_p$, neglecting the curvature at low particle velocities. The specific fit is based on Carter and Marsh's data for Shell Epon 828.[1]

The shock properties of epoxy-based alumina composites have been presented in the literature.[5,6,9–16] Addition of alumina filler particles has resulted in lowered compressibility for the composite compared to the polymer itself, with increasing volume fraction of filler resulting in additional decreases in compressibility.[5,14] The propagated waves in these materials have been observed to be rounded in certain pressure regimes,[9,15] and measured wave profiles transition from viscoelastic behavior at high input stresses to a more complex response at low input stresses due to the temporal dynamics of viscous mechanisms.[12] Additionally, samples with smaller particle sizes were shown to have steeper wave profiles indicating that viscous processes are less significant.[15] The release wave is observed to be a strong function of particle velocity[5,9] and filler volume fraction[15] and much faster than the initial shock wave.[5,9] This unexpectedly large release wave velocity has been attributed to contact stresses between the alumina particles during loading and unloading.[12]

From Setchell and Anderson,[12] the dissipative mechanisms in filled epoxy are related to the microstructure of irregular particles in a matrix. In the alumina-epoxy composite in,[12] the Al_2O_3 particles are surrounded by epoxy, whose larger compressibility should dominate the properties of the composite in shock loading. The dominance of the binder over the mechanical properties of composites has been observed,[17,18] when there is enough binder to coat the particles.[19] Setchell and Anderson[12] propose that particle spacing would be disproportionately reduced and reorienta-

a)Electronic mail: jennifer.jordan@eglin.af.mil.

tion of the particles may be required prior to equilibrium, which would account for the high release wave velocity in similar composites.[12,20] Studies of alumina-epoxy composites tested at different starting temperatures[6] have shown that the dissipative mechanism in these composites are the viscous forces in the epoxy opposing the particle motion during compression.[12]

The complexity of these composites increases when more than one particulate phase is added such as in aluminum-iron oxide-epoxy.[20–22] It was observed that the rise to peak stress in this composite was faster in the propagated wave than in the incident wave, indicating that the higher shock impedance particles decrease viscoelastic effects even further and give rise to a higher overall wave velocity from the addition of a second, high impedance filler. In addition, a step was observed on both the incident and propagated pressure traces, which may be due to the viscoelastic–viscoplastic behavior of the epoxy binder. Two volume fractions of particles have been studied, and it was found that increasing the particle concentration increased the observed shock pressure at a given particle velocity, as expected.[20]

The ability to predict the behavior of these composites from the properties of the constituents is valuable. Varying the concentrations of the constituents can tune the properties of the composites. Modeling the behavior of the composite using the properties of the constituents can greatly reduce the number of experiments needed to validate the Hugoniot. Baer *et al.*[23,24] have developed a simple model for two-phase composite materials based on the properties of the constituents. This model has been expanded to allow for any number of phases in composite materials, and the details are presented in Ref. 25. More complex microstructure based models have been developed and can be used to predict wave propagation in these complex materials.[11,26–28]

Here, we report a series of gas gun- and high explosive-driven experiments aimed at defining the equation of state of an aluminum-manganese dioxide-epoxy composite. The experimental data points are compared with both the Baer mixture model for a three phase material[25] and the mesoscale calculations performed by Fraser *et al.*[28] The behavior of the composite is found to be linear in the shock velocity-particle velocity plane for a broad range of pressures, with curvature at low particle velocities. A comparison between the data derived from gas gun-and explosive-driven plate impact experiments is given. The data also represent a successful application of embedded electromagnetic gauges in a metal-loaded composite.

II. EXPERIMENTAL PROCEDURE

A. Sample preparation

Nominally spherical aluminum (~20 μm) and irregularly shaped manganese dioxide (−60+230 mesh) powder were obtained. The powders were blended into Epon 826 according to the following volume fractions: 0.2377 Al, 0.3108 MnO_2, and 0.4515 epoxy and cured with diethanolamine. The material was cast into blocks from which appropriate samples were machined. The samples were characterized to determine their density and acoustic wave speed, given in Table I and microstructure, shown in Fig. 1. The longitudinal and shear ultrasonic wave speeds in the epoxy and the composite were measured using a GE Panametrics 25 HP Plus ultrasonic thickness gauge with a 2.25 MHz M106 transducer (longitudinal wave speed) and a 1.0 MHz V153 transducer (shear wave speed).

TABLE I. Density and longitudinal (C_l), shear (C_s), and bulk (C_0) sound speeds for the individual constituents, if available, and the Al–MnO_2-epoxy composite.

	Density (g/cm^3)	C_l (km/s)	C_s (km/s)	C_0 (km/s)
Aluminum	2.70	6.3	3.1	5.2
MnO_2	5.03			
Epoxy	1.19 ± 0.01	2.59 ± 0.01	1.09 ± 0.02	2.27
Al–MnO_2-epoxy	2.60 ± 0.02	3.36 ± 0.04	1.81 ± 0.01	2.63

B. Single stage gas gun loading experiments

Four gas gun-driven equation of state experiments were conducted at NSWC-Indian Head using the 102 mm diameter single stage light-gas gun at impact velocities between 275 and 1080 m/s, Table II. Owing to the large internal diameter of the launch tube, three samples were able to be loaded under identical conditions. The experiments, shown schematically in Fig. 2, were instrumented with piezoelectric pins used to measure time of arrival, and Bauer piezoelectric polyvinylidene fluoride (PVDF) stress gauges[29] obtained from Ktech Corporation, Albuquerque, NM or manganin

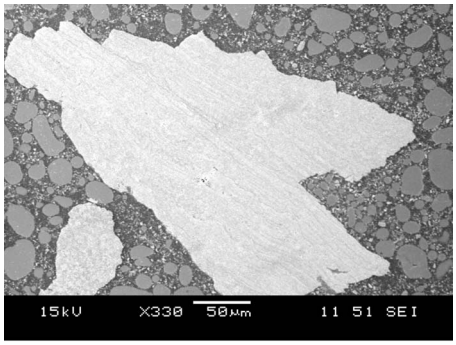

(a)

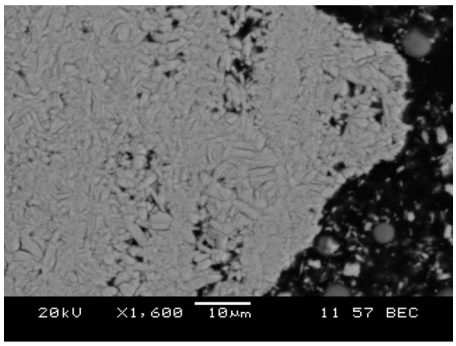

(b)

FIG. 1. Microstructure of Al–MnO_2-epoxy composite showing (a) spherical aluminum particles and irregular MnO_2 particles and (b) MnO_2 particles are comprised of small elliptical particles.

TABLE II. Details and experimental results for single stage gas gun loading experiments, where the shaded values indicate properties measured during the experiment and I indicates data from the incident gauge and (T) indicates data from the transmitted gauge. Errors on projectile velocities are <1%.

Expt. No.	Impactor	Donor	Projectile velocity (km/s)	Shock velocity (km/s)	Interface particle velocity (km/s)	Particle velocity (km/s)	Pressure (GPa)	V/V_0
JJH28	6061-T6 Al	6061-T6 Al	0.276	2.90 ± 0.15		0.18 ± 0.03	1.3 ± 0.1 (I) 1.02 (T)	
1S-1409	Al–MnO_2-epoxy	LiF	0.427	3.36	0.161	0.266	2.28	0.921
JJH120	6061-T6 Al	6061-T6 Al	0.517	3.64 ± 0.13		0.32 ± 0.06	3.0 ± 0.6	
JJH121	OFHC Cu	6061-T6 Al	0.508	3.88		0.48 (manganin) 0.41 (PVDF)	4.8 ± 0.1 (I) 3.4 ± 0.7 (T) 4.2 ± 0.2 (I)	
JJH122	OFHC Cu	OFHC Cu	0.519	3.93		0.48	4.9 ± 0.2 (I) 4.1 ± 1.8 (T)	

gauges obtained from Dynasen, Goleta, CA. The gauges were mounted between the donor and the sample and between two sample disks. An aluminum projectile with an aluminum or copper flyer plate (12.7 mm nominal thickness) was used to impact an aluminum or copper driver plate (6.73 mm nominal thickness).

The gauge mounted between the driver and the sample provides an "input" stress profile, and the gauge mounted between the two sample disks provides the "propagated" stress profile. The PVDF gauge data was reduced using PlotData from Sandia National Laboratories, with the gauge calibrations built into the software. The manganin gauge data was reduced according to the procedure discussed in Ref. 30. In order to accomplish the calibration, a decade resistance box was placed in the same position as the experimental manganin gauge. The resistance on the decade box was changed to simulate the change in resistance due to the manganin gauge and the corresponding change in voltage was recorded in order to create a calibration curve for each gauge.

An additional single stage gas gun-driven experiment was performed at Los Alamos National Laboratory (LANL) using a 78 mm bore light gas gun.[31] An ~43 mm diameter × 4.42 mm thick disk (hand polished flat) of the composite was mounted in the front of a Lexan projectile, mounted on a brass sabot, and impacted into a LiF window at 0.427 km/s. Dual VISAR measurements were recorded at the sample-LiF interface, and the Hugoniot locus was determined from the measured interface particle velocity, the known Hugoniot for LiF, and impedance matching methods.

C. Two stage gas gun loading experiments

A series of plate impact experiments were performed at LANL using a two stage (50 mm bore) light gas gun (He gas, wrap around breech) described previously.[31,32] The experiments were performed in two different ways—plate impact of a polymer impactor onto an instrumented composite target containing embedded electromagnetic gauges, and impact of projectile-mounted epoxy composite into a LiF window, with measurement of the interface particle velocity using dual velocity interferometer system for any reflector (VISARs). The large bore of the gun allows for longer recording times for one-dimensionality of the experiment. Projectile velocities were measured using a velocity-measuring system consisting of four laser diodes with four collection lenses coupled to fiber optics and photodiode detection, mounted at the end of the gun barrel. This method allows accuracy in determination of the projectile velocity to a few meter per second, usually less than 0.1%.

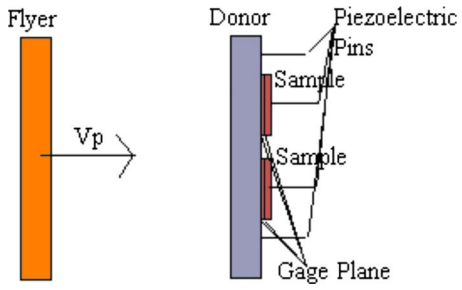

FIG. 2. (Color online) Schematic of Indian Head gas gun experiments.

Three gas gun-driven plate impact experiments were performed by launching Lexan projectiles with Kel-F 81 (polychlorotrifluoroethylene, $\rho_0 = 2.14$ g/cm^3) impactors installed in the projectile fronts at instrumented targets containing electromagnetic gauges. The maximum impact velocity achieved in these experiments ranged from 2.269 to 3.214 km/s. An electromagnetic gauging method[32–35] was used for the measurement of *in situ* shock wave profiles, from which both particle and shock velocity were directly determined. The embedded gauge package consists of 5 μm thick aluminum foil gauge pattern sandwiched and glued between two 25 μm thick FEP-Teflon membranes making an ~60 μm thick package. The voltage developed by the gauge moving in a magnetic field is directly proportional to the gauge length, magnetic field strength, and mass velocity in the material (gauge) under shock loading, according to Faraday's law.[32] The magnetic field was produced by an electromagnet mounted in the gun target chamber and produced a magnetic field strength of approximately 1.2 kG in these experiments. General schematics of the target assembly and impact geometry are shown in Fig. 3.

To meet planarity tolerances for plate impact experiments, the samples were hand polished using successfully finer grit paper with water as a lubricant. Once the desired flatness of the target pieces was achieved, an embedded gauge package was glued between the top and bottom pieces of a nominally 2 in. diameter right cylinder on a 30° angle as depicted in Fig. 4(b). This geometry allows for the distribution of the nine particle velocity gauges or "trackers" and three shock trackers in the package at known depths in the

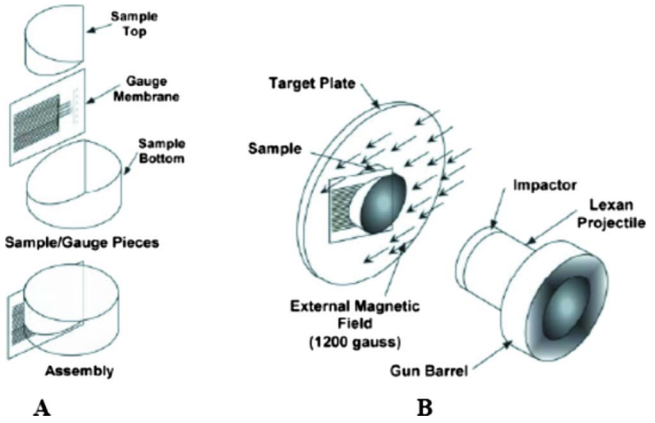

FIG. 3. (Color online) (a) Expanded view of target assembly for embedded gauge plate impact experiments and (b) schematic of the experimental target arrangement with respect to the magnetic field and projectile/impactor at the LANL Chamber 9 facility.

sample relative to the impact face. The nine horizontal foils down the center of the package, Fig. 4(a), are the particle velocity trackers, and provide an *in situ* measurement of mass velocity at discrete, known Lagrangian positions within the target. The finely patterned "shock trackers" are on each side of the particle velocity trackers and at the bottom center of the package. The shock trackers provide a large number of well-spaced foils to allow for accurate and redundant determination of the shock velocity in the material. Insertion at an angle allows the gauges not to shadow one another, producing a condition of minimum perturbation. After gluing the embedded gauge between the two target pieces, Fig. 4(b), additional polishing of the target face was performed to create a flat impact surface. A single element foil gauge, referred to as a "stirrup" gauge was then affixed to the impact face, Fig. 4(c). Particle (mass) velocity (u_p) was obtained from the peak voltage of the impact face mounted electromagnetic gauge. The shock velocity (U_s) was redundantly determined from measured gauge positions and the arrival time of the shock at nine particle velocity trackers and three shock trackers in the gauge element.

The presence of metal particles in the target was a concern when applying the embedded electromagnetic gauge method. To confirm that the gauge response was unperturbed by the Al and MnO_2 loading in the samples, dual VISARs were fielded at the back of a target:LiF interface for Shot 2S-318. The particle velocity at the rear interface was as expected from impedance matching calculations. To further confirm that the response of the electromagnetic gauges was not influenced by the metal particles in the composite, two additional experiments were performed on the two-stage gun in which the composite was mounted in the front of the projectile, and impacted into a LiF window. The experimental configuration was the same as described above for the single stage gas gun experiment at LANL. Again, dual VISAR signals were recorded at the sample-LiF interface, and the Hugoniot locus was determined from the measured interface particle velocity, the known Hugoniot for LiF, and impedance matching methods.

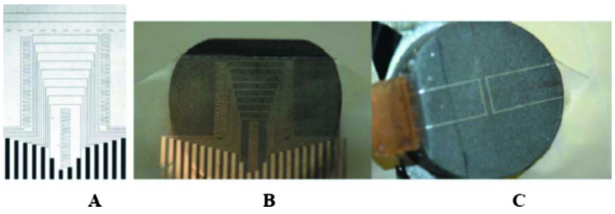

FIG. 4. (Color online) (a) Optical micrograph of embedded gauge package. The package consists of 5 μm thick Al patterned and sandwiched between layers of FEP-Teflon membrane. (b) The gauge membrane glued to the target bottom. (c) The fully assembled target showing the single element stirrup gauge on the target impact face.

D. Explosive loading experiments

Fourteen experiments, detailed in Table IV and shown schematically in Fig. 5, were conducted at Eglin AFB using explosive plane wave lenses (PWL) to generate shock loading at higher pressures. In these experiments, the PWL was in contact with an explosive pad of Baratol, TNT, or 75/25 Octol (25.4 mm thick) to generate a range of pressures in a 6061-T6 aluminum (Al) or OFHC copper (Cu) donor plate.

In explosive loading experiments, the shock wave travels from the donor to the sample. The shock velocity in the Al or Cu donor material and the sample was measured using piezoelectric pins (Dynasen CA-1135), which were placed in holes drilled into the sample at differing depths. Using the shock velocity in the donor plate and the sample, the remaining Hugoniot properties for the sample were determined using impedance matching.

Initial experiments JJH15—16, Fig. 5(a), were conducted in which the shock velocity in the sample and metal plate were measured simultaneously. In these experiments, nine piezoelectric pins were used. Calibration shots were performed in order to understand the explosive-metal interaction and are discussed in detail in Ref. 16. After the calibration shots were conducted, a new experimental design was implemented in which two samples are tested simultaneously, shown in Fig. 5(b), and additional experiments were conducted (JJH54–65) in which Al–MnO_2-epoxy was one of the samples. The known explosive-donor interaction from the calibration shots is used for impedance matching to the donor properties.

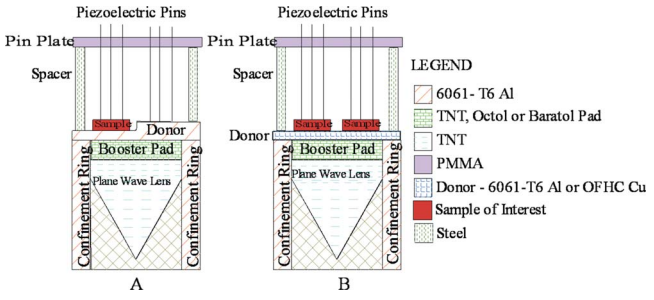

FIG. 5. (Color online) Schematic of explosive loading experiments showing (a) first revision measuring shock velocity in sample and metal donor (JJH15–16) and (b) second revision measuring shock velocity in two samples (JJH54–65).

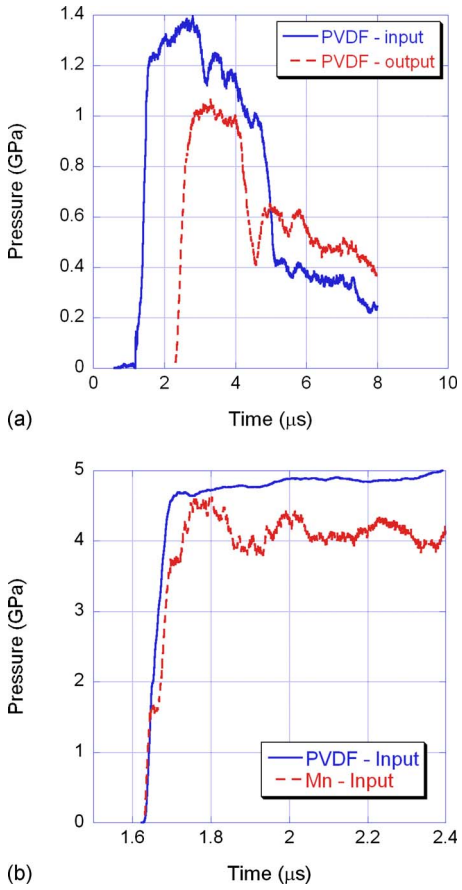

FIG. 6. (Color online) (a) Experiment JJH28 PVDF gauge traces and (b) experiment JJH121 PVDF and manganin input gauge traces.

III. RESULTS

A. Single stage gas gun experiments

Five single stage gas gun loading experiments were conducted in total, four at NSWC (JJH28 and JJH120–122) and one at LANL (1S-1409), and the results are given in Table II. In the NSWC gun experiments, the shock velocity was measured using gauges and time of arrival pins. The experiments had PVDF gauges in all experiments and manganin gauges in JJH121 and 122. However, data acquired from the gauges was not usable in every case. In JJH120, the shock velocity was determined by the piezoelectric time of arrival pins, and the error reported is the variation among the pins. For JJH120, the gauge data was not able to be reduced, so the shock state in the composite was determined by impedance matching to the donor plate. The aluminum donor shock state was determined by impedance matching to the flyer with the measured impact velocity.

In JJH28, both the input and transmitted PVDF gauges were able to be reduced and are shown in Fig. 6(a). The shock velocity in JJH28 was calculated from the arrival time at both gauges and the time of arrival pins. Additionally, the peak pressures from the input and transmitted gauges are given in Table II. The peak pressure was determined by averaging the plateau, with the error reported the deviation from that average. In the case of the input gauge where the pressure is continuously rising over the peak plateau, the average over the whole plateau was used. It can be seen that the pressure recorded on the transmitted gauge is less than that recorded on the input gauge, which has also been observed in aluminum-iron oxide-epoxy composites.[22] This experiment is at low pressures, in the regime where epoxy is undergoing viscoelastic compressive behavior, and this may account for the decreased transmitted stress, which is not seen in higher pressure two-stage gas gun experiments.

In JJH121, both PVDF and manganin gauge traces were recorded. The input traces are shown in Fig. 6(b). The shock velocity was calculated from the arrival times at the input and transmitted manganin gauges. There are two elbows in the manganin gauge trace, which could be due to reverberations in the gauge as it rings up. Additionally, the plateau has a periodic structure, which may be due to the gauge picking up electrical noise. The transmitted manganin signal is extremely noisy probably due to the failure of the input gauge. Greenwood, *et al.*[36] have shown that selection of a proper electrical circuit can minimize this noise during gauge failure. There is a small difference in the peak pressure seen in the PVDF and manganin gauges. These gauges were between the donor plate and the sample in the same experiment; however, they are not physically at the same location, but are mounted between two different samples and the donor plate. The difference in peak pressure may be due to the composite nature of the samples, which could result in slightly different material compositions in the region of the gauges.

In experiment JJH122, the shock velocity and peak pressure were calculated from manganin gauge data, where there was a periodic structure on the input gauge, which may be due to ringing in the gauge itself. The transmitted gauge showed considerable noise. Again, this could be corrected with an electrical circuit on the input gauge to prevent its failure being seen on the transmitted gauge.

For the front surface impact experiment, 1S-1409, conducted at LANL, the shock wave profile at the composite-LiF interface exhibited heterogeneity in the flat top, likely due to the composite nature of the sample. The velocity dispersion in the wave profile at the top was on the order of 2%–3% and the average velocity was taken for the calculation of the Hugoniot locus in Table II.

B. Two stage gas gun experiments

Three plate impact experiments were performed over a range of impact velocities designed to cover the range of pressures achieved in the explosive loading experiments using electromagnetic gauges. Both the particle and shock velocities are measured directly and redundantly in the experiments, i.e., no impedance matching methods are used. Particle and shock velocities are derived from the response of the stirrup and embedded electromagnetic gauges under shock loading, with the target sitting in a magnetic field.

The response of the stirrup gauge was used to determine u_p with all of the particle velocity gauges providing dynamic wave profiles through the sample and corroborating the results for u_p determination. Figure 7 shows the response of the embedded gauges for shot 2S-333. It can be seen that the particle velocity achieved in this gauge appears to be con-

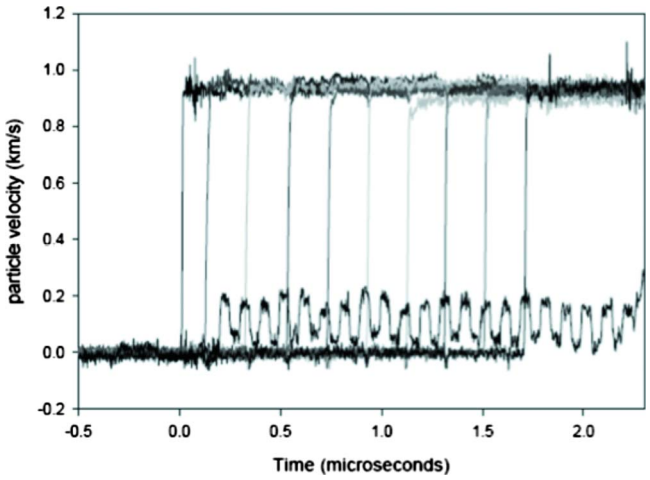

FIG. 7. (Color online) Corrected response of nine particle trackers and one, of the three, shock velocity trackers for experiment 2S-333. The Hugoniot point was determined from the particle velocity of the impact face gauge and shock velocity from the shock arrival at the nine particle velocity and three shock velocity trackers at their respective Lagrangian positions in the sample.

stant throughout the length of the sample, which differs from the attenuation seen in the PVDF gauge measurements [Fig. 6(a)]. This experiment (2S-333) is conducted at much higher pressure, in the linear region of the epoxy shock equation of state, which is the most likely explanation for the difference.

The rise and top of the wave profile were fit to linear functions with their intersection taken as the material's particle velocity. The arrival times of the shock wave at the embedded shock and particle velocity gauges as a function of Lagrangian position in the sample were used to derive U_s. A summary of the measured Hugoniot points for this experimental technique is presented in Table III.

The remaining two plate impact experiments were performed at impact velocities necessary to generate particle velocities to span those measured using the single stage gas gun and explosive loading techniques. Table III summarizes the results of the three experiments, including the calculated hydrodynamic pressures and specific volumes from the conservation equations

$$P = \rho_0 U_s u_p \tag{1}$$

$$\frac{V}{V_0} = 1 - \frac{u_p}{U_s} \tag{2}$$

C. Explosive loading experiments

Fourteen explosive loading experiments were conducted and are listed in Table IV. The donor shock velocity was determined from the average shock velocity measured in 2–3 experiments. In all experiments, the time of arrival of the shock wave in the sample was determined using piezoelectric pins at different depths. For each sample, there were two pin concentric pin circles. The pins were measured in groups of three pins at different heights. The shock velocity for each pin group was determined and the shock velocity for the sample was then calculated as the average of the ping groups. The variability in this experimental technique is evident from the difference between identical experiments, with the average deviation in shock velocity being ± 0.1 mm/μs. The remaining properties in the composite are determined from impedance matching to the donor and the conservation equations.

IV. DISCUSSION

Highly-filled polymer composites are a class of materials that are garnering growing attention due to their combination of light mass and high strength for use in structural and related engineering components. Plastic-bonded explosives and related energetic materials are members of this class of materials that also have received growing interest because of recent advances in high precision material preparation and formulation, including micron-scale resolution characterization of microstructures. Here, we have examined the dynamic (shock) compressive properties of a three-component polymer composite consisting of Al–MnO_2-epoxy composites, which builds upon the wealth of literature reports on related ALOX (Refs. 5, 6, and 9–16) and Al–Fe_2O_3-epoxy composites.[20–22] The results described in this work feed into multi-phase equation of state models being developed by this team and others, in efforts to predict the shock response of multi-phase composites from knowledge of the equation of state properties of the individual constituents.[25–28,37,38]

The Hugoniot loci determined from the 4 types of shock compression experiments between three laboratories are shown collectively in Fig. 8. Also shown in the figure is the bulk sound speed, $c_b = 2.631$ km/s, determined from ultrasonic measurements at AFRL at ambient conditions. Overall, there is good agreement between the Hugoniot points determined by the different methods, between different laboratories. The data span the range of particle velocities from 0.18–1.75 km/s or, equivalently, pressures from 2.3 to 28.4 GPa.

TABLE III. Details and experimental results for two stage gas gun loading experiments, where the shaded values indicate properties measured during the experiment. Errors on projectile velocity are <1%, while errors on measured shock and particle velocities are within 1%–2%.

Expt. No.	Expt. type	Projectile velocity (km/s)	Shock velocity (km/s)	Interface particle velocity (km/s)	Particle velocity (km/s)	Pressure (GPa)	V/V_0
2S-333	Embedded gauge	2.269	4.978	N/A	0.9239	12.0	0.813
2S-371	Front surface impact	2.005	5.22	0.900	1.105	15.1	0.788
2S-336	Embedded gauge	2.770	5.333	N/A	1.1720	16.3	0.780
2S-318	Embedded gauge	3.214	5.578	N/A	1.3650	19.9	0.755
2S-372	Front surface impact	3.249	6.19	1.500	1.750	28.4	0.717

TABLE IV. Details and experimental results for explosive loading experiments, where the shaded values indicate properties measured during the experiment.

Expt. No.	Explosive	Donor	Donor shock velocity (km/s)	Shock velocity (km/s)	Particle velocity (km/s)	Pressure (GPa)	V/V_0
JJH64	Baratol	Copper	4.48 ± 0.14	4.08	0.56	6.0	0.86
JJH65	Baratol	Copper		4.18	0.56	6.1	0.87
JJH56	TNT	Copper	4.56 ± 0.01	4.14	0.65	7.0	0.84
JJH57	TNT	Copper		4.26	0.64	7.1	0.85
JJH16	Baratol	Aluminum	6.31 ± 0.04	4.98	0.82	10.6	0.84
JJH62	Baratol	Aluminum		4.81	0.83	10.3	0.83
JJH63	Baratol	Aluminum		4.52	0.85	10.0	0.81
JJH60	Octol	Copper	4.87 ± 0.25	4.87	0.94	11.9	0.81
JJH61	Octol	Copper		5.05	0.94	12.3	0.81
JJH54	TNT	Aluminum	6.63 ± 0.04	5.29	1.08	14.9	0.80
JJH55	TNT	Aluminum		5.10	1.10	14.6	0.78
JJH15	Octol	Aluminum	7.31 ± 0.10	5.30	1.73	23.8	0.67
JJH58	Octol	Aluminum		5.41	1.71	24.1	0.68
JJH59	Octol	Aluminum		5.36	1.72	23.9	0.68

In the shock velocity-particle velocity plane, Fig. 8(a) the Rankine—Hugoniot behavior is nominally linear and does not show any evidence of phase transitions. Further inspection of the wave profiles reveal unreacted behavior. As seen in Fig. 7, the shock wave profiles recorded at each of ten particle velocity gauge positions for 2S-333 are flat, with a rapid rise time, reaching peak particle velocity within ~20 ns. Figure 9 shows shock wave profiles recorded with dual VISARs at the composite-LiF interface for shot 2S-371, in which the composite was impacted into LiF at 2.005 km/s. The wave profiles show some roughness, or velocity variations, at the peak state, likely related to the heterogeneity of the material and the high fill percentages of two types of filler particles in the sample. The wave profiles from both embedded gauges and VISAR measurements do not show any evidence of shock-induced phase transformation or reactions under uniaxial compression and to calculated hydrodynamic pressures exceeding 20 GPa. In addition, the consistency of the wave profiles through the sample and the magnitude of the measured particle velocity using the electromagnetic gauges indicate the sample remained nonconductive during the test. Interestingly, the shock wave profiles do not show any substantial shape evolution as the shock traverses the sample, regardless of input pressure between ~2.3 and 20 GPa. This is in contrast to what was observed by Anderson, *et al.*[5] for ALOX using VISAR and PVDF gauge measurements 6 mm into filled epoxy targets, in which the wave profiles showed considerable rounding and dispersion. However, this polymer composite is much more highly loaded than any of those tested by Anderson *et al.*[5] Typically, polymers show viscoelastic responses at low shock input pressures, as evidenced by a rounded shock wave front.[39,40]

A down turn, or curvature, in the data in the shock velocity-particle velocity plane at low particle velocities has also been observed for many polymers. Carter and Marsh[1] attribute this to be due to two-dimensional compressibility at low pressures, where spacing between polymer chains is decreasing, but the chain length remains relatively constant. More recently, Clements[39] has developed a rate-dependent volumetric viscoelastic approach to describe this behavior. Curvature in this plane is observed for the filled composite below $u_p \sim 0.7$ km/s, Fig. 8(a), with a linear Rankine–Hugoniot fit overestimating the bulk sound speed.

A linear fit to the experimental data derived from two stage gas gun-driven plate impact and explosive loading experiments between $0.7 \leq u_p \leq 1.7$ km/s yields the following relationship

$$U_s = 1.47 \times u_p + 3.61 \tag{3}$$

which extrapolates to a value much higher than the ultrasonic bulk sound speed and does not capture the low pressure shock data in this plane. A more satisfactory fit to the data in this plane is the quadratic form:

$$U_s = 2.64 + 2.86 \times u_p - 0.48 \times u_p^2 \tag{4}$$

The curvature in this plane may be attributed to a combination of viscoelastic effects, compaction of porosity in the composite, and the disparity in shock impedances (and possibly physical contact) between the multiple phases of the composite.

Additionally, epoxy exhibits a high pressure cusp in the $U_s - u_p$ plane at 23.1 GPa.[1] We have observed differences and scatter in the gas gun versus explosive-driven experimental data in this regime. However, additional higher pressure experiments are required to confirm decomposition or chemistry in this regime, preferably with *in situ* measurements of shock wave profiles.

Figures 8(b) and 8(c) shows the same data in the pressure-particle velocity and pressure-volume planes, respectively. The fits to the experimental data determined in the $U_s - u_p$ plane are included. As in the $U_s - u_p$ plane, the quadratic fit to the experimental data is a better match, particularly in the P-V/V_0 plane. The difference in the experimental data between the gas gun and explosive driven experiments at high pressures is prominent in the P-V/V_0 plane. This discrepancy occurs close to the high pressure cusp determined by Carter and Marsh for epoxy.[1] Again,

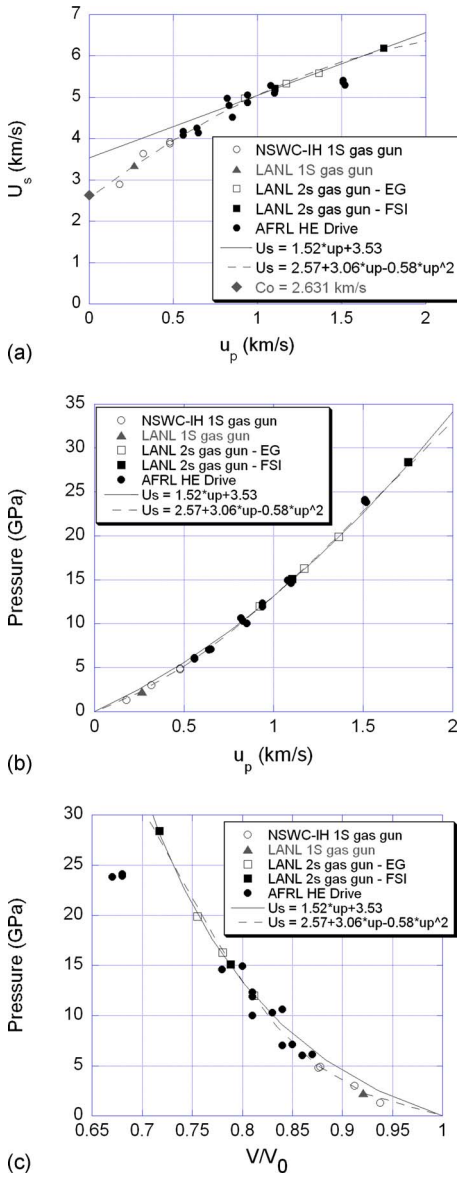

FIG. 8. (Color online) (a) Shock velocity-particle velocity, (b) pressure vs particle velocity, and (c) pressure vs volume data from Al–MnO_2-epoxy composite from the three types of experiments. The linear Rankine–Hugoniot fit to the intermediate-to-high pressure data overestimates the data at low pressures and the bulk sound speed. A more satisfactory fitting form is the quadratic equation $U_s = 2.64 + 2.86 * u_p - 0.48 * u_p^2$.

additional experiments, particularly with time resolved measurements, need to be conducted to understand this differences.

The Al–MnO_2-epoxy composite contains 45 vol % epoxy. This is the most highly loaded epoxy-based composite studied to date.[5,6,9–16,20–22] This composite shows the, expectedly, stiffer behavior compared to the other materials. Additionally, the Al–MnO_2-epoxy composite displays the down turn, or curvature, in the data in the shock velocity-particle velocity plane at low particle velocities. Other materials studied in the literature do not appear to show a pronounced downturn in the shock measurements, although the measured values do extrapolate to a value above the bulk sound speed.

The Hugoniot for the Al–MnO_2-epoxy composite was calculated using both the Baer mixture model[25] and a mesoscale model reported by Fraser, *et al.*[28] Both models used a piecewise fit for the epoxy $U_s - u_p$ relationship to account for a possible high pressure phase change. Additionally, the low pressure epoxy data was fit with a quadratic function for the Baer mixture model. The equation of state for MnO_2 was determined from that for pyrolusite, as presented in Ref. 2. The MnO_2 material displays porosity in Fig. 1(b), so that the density, and subsequently the equation of state, was modified by matching the composite mixture density to the experimentally measured composite density. The shock equation of state input parameters used for both models are presented in Table V. Both models, compared with the experimental data, are presented in Fig. 10 in the $U_s - u_p$ plane. For the given input parameters, both models underpredict the experimental data by approximately 10%. For both models, there is better agreement with the experimental data at lower particle velocities. There is uncertainty in the input parameters for the models, i.e., the constituent densities and shock equations of state, which may account for the differences between the models and the experimental data. Given the similar underprediction in both modeling methods, additional investigation of the input parameters must be conducted.

This paper presents the experimental measurement of the shock equation of state for an Al–MnO_2-epoxy composite

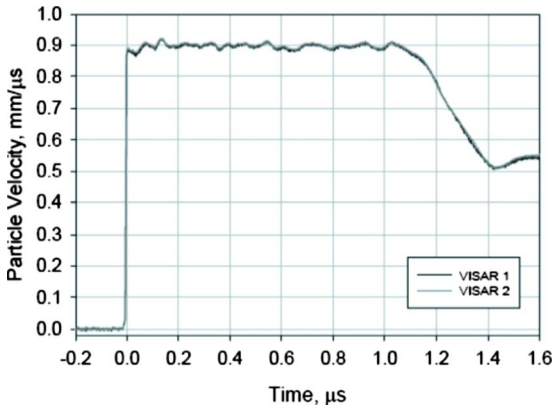

FIG. 9. (Color online) VISAR shock wave profile for shot 2S-371 measured at the LiF-sample interface.

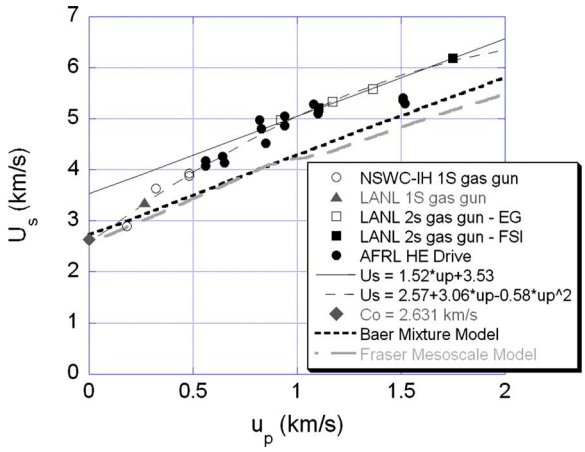

FIG. 10. (Color online) Comparison of experimental data with Baer mixture model and mesoscale model by Fraser *et al.* (Ref. 27.)

TABLE V. Input parameters for mixture and mesoscale models.

Parameter	MnO_2	Al	Epoxy phase I[a]	Epoxy phase II	Epoxy phase III	Epoxy phase IV
Density (g/cm^3)	4.55	2.70	1.19	1.19	1.19	1.19
C_0 (km/s)	3.63	5.29		2.67	7.17	2.88
S	1.52	1.37		1.55	0.01	1.35
a			−0.3947			
b			3.4704			
c			2.263			

[a]Only used in mixture model.

between 1.3 and 28 GPa. The high pressure phase transformation in epoxy was not observed in these experiments. Additional work measuring the *in-situ* wave profiles at high pressure should be accomplished to probe the decomposition/chemical reactions in the epoxy. Additional low pressure experiments should be conducted to probe the rounding due to viscoelastic effects in this highly loaded material. Finally, calculation of multi-phase equations of state should be further investigated to include uncertainties in the input parameters for the constituents.

V. CONCLUSIONS

The shock equation of state for Al–MnO_2-epoxy particulate composite was determined using three loading techniques—single stage light gas gun, two stage light gas gun, and explosive loading. The Rankine–Hugoniot ($U_s - u_p$) relationship was found to be linear for a portion of the particle velocity space between $0.7 \leq u_p \leq 1.7$ km/s. A better representation of the data was found with a quadratic function, $U_s = 2.64 + 2.86 \times u_p - 0.48 \times u_p^2$, due to significant curvature in this plane. Deviations from linearity at low particle velocities may be attributed to a combination of viscoelastic effects, compaction of porosity in the composite (or disparate inter-and intramolecular forces and free volume), and dissimilar shock impedances (and possibly spatial contact) of the multiple phases of the composite. Scatter in the data at high pressures/particle velocities may be due to transition between the reactants and products caused by shock-induced chemistry and decomposition in the epoxy binder. However, additional experiments are needed to elucidate these phenomena. The quadratic fit determined from the $U_s - u_p$ data provides an excellent fit to the data in the P-V/V_0 and P-u_p planes.

ACKNOWLEDGMENTS

The authors would like to acknowledge the help of several people and groups who assisted in the construction, setup, and implementation of the experiments—Mr. Mark Grimmonpre (AFRL), Mr. Ricky Beesley (AFRL) and Mr. Mark Johnson (AFRL), AFRL/RW Processing Section, Mr. Alan Zakarais (NSWC-IH), Mr. Grant Rogerson (NSWC-IH), and Mr. Andrew Fraser (NSWC-IH and Marquette University). Dr. John Borg and Mr. Andrew Fraser (Marquette University) provided helpful information regarding mesoscale modeling. The authors would also like to thank Dr. Jerry Forbes for useful insights and discussions. This research was sponsored by AFRL/RWME. Opinions, interpretations, conclusions, and recommendations are those of the authors and not necessarily endorsed by the United States Air Force.

[1]W. J. Carter and S. P. Marsh, "Hugoniot Equation of State of Polymers," Los Alamos National Laboratory Report No. LA-13006-MS (Los Alamos National Laboratory, Los Alamos, NM, 1995).
[2]*LASL Shock Hugoniot Data*, edited by S. P. Marsh (University of California Press, Berkeley, 1980).
[3]D. E. Munson and R. P. May, J. Appl. Phys. **43**, 962 (1972).
[4]J. C. F. Millett, N. K. Bourne, and N. R. Barnes, J. Appl. Phys. **92**, 6590 (2002).
[5]M. U. Anderson, R. E. Setchell, and D. E. Cox, in *Shock Compression of Condensed Matter—1999*, edited by M. D. Furnish, L. C. Chhabildas, and R. S. Hixson (American Institute of Physics, Melville, NY, 2000), pp. 551–554.
[6]M. U. Anderson, R. E. Setchell, and D. E. Cox, in *Shock Compression of Condensed Matter—2001*, edited by M. D. Furnish, N. N. Thadhani, and Y. Horie (American Institute of Physics, Melville, NY, 2002), pp. 669–672.
[7]C. E. Morris, J. N. Fritz, and R. G. McQueen, J. Chem. Phys. **80**, 5203 (1984).
[8]C. E. Morris, E. D. Loughran, G. F. Mortensen, G. T. I. Gray, and M. S. Shaw, *Shock induced dissociation of polyethylene, APS Topical Conference on Shock Compression of Condensed Matter* (Elsevier, Amsterdam, 1990).
[9]D. E. Munson, R. R. Boade, and K. W. Schuler, J. Appl. Phys. **49**, 4797 (1978).
[10]L. C. Chhabildas and J. W. Swegle, J. Appl. Phys. **53**, 954 (1982).
[11]D. S. Drumheller, J. Appl. Phys. **53**, 957 (1982).
[12]R. E. Setchell and M. U. Anderson, J. Appl. Phys. **97**, 083518 (2005).
[13]M. U. Anderson, D. E. Cox, S. T. Montgomery, and R. E. Setchell, in *Shock Compression of Condensed Matter—2005*, edited by M. D. Furnish, M. Elert, T. P. Russell, and C. T. White (American Institute of Physics, Melville, NY, 2006), pp. 789–792.
[14]J. C. F. Millett, N. K. Bourne, and D. Deas, J. Phys. D **38**, 930 (2005).
[15]R. E. Setchell, M. U. Anderson, and S. T. Montgomery, J. Appl. Phys. **101**, 083527 (2007).
[16]J. C. F. Millett, D. Deas, N. K. Bourne, and S. T. Montgomery, J. Appl. Phys. **102**, 063518 (2007).
[17]J. L. Jordan, C. R. Siviour, D. W. Richards, C. G. Rumchik, and R. D. Dick, *Proceedings of the 2005 SEM Annual Conference and Exposition on Experimental and Applied Mechanics* (Society for Experimental Mechanics, Bethel, CT, 2005), pp. 81–90.
[18]J. L. Jordan, B. White, J. E. Spowart, D. W. Richards, and N. N. Thadhani, *Proceedings of the SEM Annual Conference and Exposition on Experimental and Applied Mechanics 2007* (Society for Experimental Mechanics, Bethel, CT, 2007), Vol. 3, pp. 1968–1978.
[19]C. G. Rumchik and J. L. Jordan, in *Shock Compression of Condensed Matter—2007*, edited by M. Elert, M. D. Furnish, R. Chau, N. Holmes, and J. Nguyen (American Institute of Physics, Melville, NY, 2007), pp. 795–798.
[20]L. Ferranti, "Mechanochemical Reactions and Strengthening in Epoxy-Cast Aluminum Iron-Oxide Mixtures," Ph.D. Dissertation, Georgia Institute of Technology (2007).
[21]L. Ferranti, J. L. Jordan, R. D. Dick, and N. N. Thadhani, in *Shock Compression of Condensed Matter—2007*, edited by M. Elert, M. D. Furnish, R. Chau, N. Holmes, and J. Nguyen (American Institute of Physics, Melville, NY, 2007), pp. 123–126.
[22]J. L. Jordan, L. Ferranti, R. A. Austin, R. D. Dick, J. R. Foley, N. N.

Thadhani, D. L. McDowell, and D. J. Benson, J. Appl. Phys. **101**, 093520 (2007).
[23]M. R. Baer and J. W. Nunziato, Int. J. Multiph. Flow **12**, 861 (1986).
[24]M. R. Baer, C. A. Hall, R. L. Gustavson, D. E. Hooks, and S. A. Sheffield, J. Appl. Phys. **101**, 034906 (2007).
[25]J. L. Jordan, D. Dattelbaum, L. Ferranti, G. Sutherland, M. Baer, W. Richards, S. Sheffield, R. D. Dick, and N. N. Thadhani, *Shock Compression of Condensed Matter* (American Institute of Physics, Melville, NY, 2009).
[26]R. A. Austin, D. L. McDowell, and D. J. Benson, Model. Simul. Mater. Sci. Eng. **14**, 537 (2006).
[27]D. E. Eakins and N. N. Thadhani, Acta Mater. **56**, 1496 (2008).
[28]A. Fraser, J. P. Borg, J. L. Jordan, and G. Sutherland, *Proceedings of the SEM Annual Conference* (Society for Experimental Mechanics, Bethel, CT, 2009).
[29]F. Bauer, U.S. Patent No. 4684337 (1987).
[30]"Piezoresistive Pulse Power Supply Model CK2-50/0.050-300 Instruction Manual," Dynasen, Inc., January (2008).
[31]S. A. Sheffield and R. R. Alcon, Shock Compression of Condensed Matter **1991**, 909 (1992).
[32]S. A. Sheffield, R. L. Gustavsen, and R. R. Alcon, in *Situ Magnetic Gauging Technique used at LANL—Method and Shock Information Obtained,"* *Shock Compression of Condensed Matter—1999*, edited by M. D. Furnish, L. C. Chhabildas, and R. S. Hixson (American Institute of Physics, Melville, NY, 2000), pp. 1043–1048.
[33]V. M. Zaitzev, P. F. Pokhil, and K. K. Shvedov, DAN SSSR **132**, 1339 (1960).
[34]M. Cowperthwaite and J. T. Rosenberg, "A multiple lagrange gauge study of the shock initation process in cast TNT," Report No. ACR-223 (Office of Naval Research, Washington, D.C., 1976).
[35]C. Young, R. Fowles, and R. P. Swift, in *Shock Waves and Mechanical Properties of Solids*, edited by J. J. Burke and V. Weiss (Syracuse University Press, Syracuse, 1981).
[36]D. Greenwood, J. Forbes, F. Garcia, K. Vandersall, P. Urtiew, L. Green, and L. Erickson, in *Shock Compression of Condensed Matter—2001*, edited by M. D. Furnish, N. N. Thadhani, and Y. Horie, 2002), pp. 1157–1160.
[37]M. R. Baer, Thermochim. Acta **384**, 351 (2002).
[38]W. M. Trott, M. R. Baer, J. N. Castaneda, L. C. Chhabildas, and J. R. Asay, J. Appl. Phys. **101**, 024917 (2007).
[39]B. Clements, *Shock Compression of Condensed Matter* (American Institute of Physics, Melville, NY, 2009), pp. 1223–1228.
[40]K. W. Schuler and J. W. Nunziato, J. Appl. Phys. **47**, 2995 (1976).

DISTRIBUTION LIST
AFRL-RW-EG-TP-2010-111

*Defense Technical Info Center
8725 John J. Kingman Rd Ste 0944
Fort Belvoir VA 22060-6218

AFRL/RWOC-1 (STINFO Office)